ACS APPLIED MATERIALS & INTERFACES

Research Article

www.acsami.org

Improving Photovoltaic Performance of the Linear A-Ar-A-type Small Molecules with Diketopyrropyrrole Arms by Tuning the Linkage Position of the Anthracene Core

Xiongwei Duan,[†] Manjun Xiao,[†,‡] Jianhua Chen,[†] Xiangdong Wang,[†] Wenhong Peng,[†] Linrui Duan,[†] Hua Tan,[†] Gangtie Lei,[†] Renqiang Yang,*[,‡] and Weiguo Zhu*[,†]

[†]College of Chemistry, Xiangtan University, Key Lab of Environment-Friendly Chemistry and Application in Ministry of Education, Xiangtan 411105, China

[‡]Qingdao Institute of Bioenergy and Bioprocess Technology, Chinese Academy of Sciences, Qingdao 266101, China

Supporting Information

ABSTRACT: Two isomeric A-Ar-A-type small molecules of $DPP_2An(9,10)$ and $DPP_2An(2,6)$, were synthesized with two acceptor arms of diketopyrropyrroles (DPP) and a planar aryl hydrocarbon core of the different substituted anthracene (An), respectively. Their thermal stability, crystallinity, optoelectronic, and photovoltaic performances were investigated. Significantly red-shifted absorption profile and higher HOMO level were observed for the $DPP_2An(2,6)$ with 2,6-substituted anthracene relative to the $DPP_2An(9,10)$ with 9,10-substituted anthracene, as the former exhibited better planarity and a larger conjugate system. As a result, the solution-processing solar cells based on $DPP_2An(2,6)$ and $PC_{71}BM$ (*w*/*w*,1:1) displayed remarkably increased power conversion efficiency of 5.44% and short-circuit current density (J_{sc}) of 11.90 mA/cm^2 under 1% 1,8-diiodooctane additive. The PCE and J_{sc} values were 3.7 and 2.9 times those of the optimized $DPP_2An(9,10)$-based cells, respectively. This work demonstrates that changing the linkage position of the anthracene core in the A-Ar-A-type SMs can strongly improve the photovoltaic properties in organic solar cells.

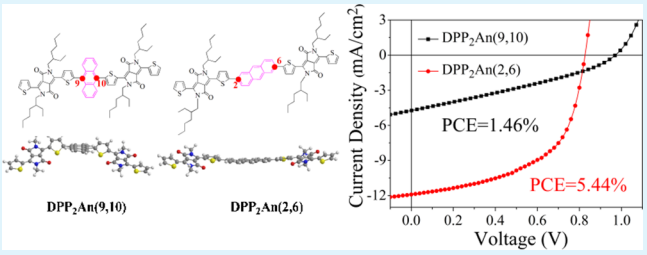

KEYWORDS: *diketopyrropyrroles, anthracene, A-Ar-A-type small molecules, photovoltaic property, organic solar cells*

1. INTRODUCTION

Solution-processed photovoltaic narrowed band gap organic small molecules (SMs) have recently been receiving increasing interest with definite molecular structure and high purity in bulk-heterojunction (BHJ) organic solar cells (OSCs), which can exhibit good batch-to-batch reproducibility.[1−6] A significant development has been made for the SMs-based OSCs with an increasing power conversion efficiency (PCE) of 10.08% through molecular design and device optimization.[7] However, compared to the well-developed photovoltaic polymeric materials, SMs still exhibit inferior photovoltaic performances in their solar cells.[3] Therefore, it is necessary to continually design new photovoltaic SMs for improving cell performance.

Generally, as a high-performance photovoltaic donor material, it should exhibit strong photo absorption in the visible region, suitable molecular orbital energy levels, high carrier mobility, excellent film morphology, and good miscibility with fullerene derivatives.[4] In order to achieve the above goal, one effective strategy is to build low band gap SMs with donor−acceptor (D−A) framework.[8] By tuning alkyls in side chains,[9−12] as well as the isomers caused by atom position,[13,14] and the linkage positions of functional groups,[15] these D−A-type donor materials exhibited some improved photoelectronic and photovoltaic properties.

In recent years, diketopyrrolopyrrole (DPP) has been used as a promising type of acceptor unit in photovoltaic SMs owing to its good planarity, intense absorption in the near-infrared region, strong electron-withdrawing property, and good photochemical stability.[16−23] The polycyclic aryl (Ar) units have also been emerged as terminal and central building blocks in the linear-type and star-type SMs because these Ar units have a good planarity and enlarged π-conjugation system, which can result in intense $\pi-\pi$ stacking and interacting tendency.[24−26] As a result, several photovoltaic SMs with a DPP_2Ar framework have been developed, which combine two DPP arms and a Ar core.[27−34] The different Ar unit exhibited significant influence on the photovoltaic property of the DPP_2Ar-type SMs. Among these, DPP_2Ar-type SMs with an aryl hydrocarbon core, one with a 2,6-naphthalene core, exhibited a high PCE of 4.4% in BHJ-OSCs.

In order to further investigate the influence of the Ar hydrocarbon core and its linkage position on photovoltaic property of DPP_2Ar-type SMs, two novel isomeric SMs of $DPP_2An(9,10)$ and $DPP_2An(2,6)$ were constructed using a

Received: April 17, 2015
Accepted: August 3, 2015
Published: August 3, 2015

DOI: 10.1021/acsami.5b03338
ACS Appl. Mater. Interfaces 2015, 7, 18292−18299

different substituted anthracene (An) unit as the Ar hydrocarbon core and two DPP units as arms. Both molecular structures are shown in Scheme 1, which contain 9,10-anthracene for $DPP_2An(9,10)$ and 2,6-anthracene units for $DPP_2An(2,6)$. As this An core has an extended π-conjugated system compared to the 2,6-naphthalene core, it should be in favor of narrowing the band gap and enhancing molecular $\pi-\pi$ stacking, finally improving the photovoltaic property. As expected, the significant influence of the aryl core and its linkage position on photoelectronic and photovoltaic properties was exhibited. Stronger photo absorption, higher hole mobility, and increasing HOMO energy level were obtained in $DPP_2An(2,6)$ rather than $DPP_2An(9,10)$. As a result, $DPP_2An(2,6)$ showed better photovoltaic performance compared with $DPP_2An(9,10)$ in the solution-processed BHJ-OSCs. The increasing PCE of 5.44% short-circuit current density (J_{sc}) of 11.90 mA/cm^2 and a fill factor (FF) of 55.40% were obtained in the optimized $DPP_2An(2,6)$-based cells using $PC_{71}BM$ as acceptor component. This PCE value was 3.7 times that of the optimized $DPP_2An(9,10)$-based cells. To the best of our knowledge, this PCE value is one of the highest levels among these DPP_2Ar-type SMs with Ar hydrocarbon core in BHJ-OSCs.

Scheme 1. Molecular Structures of $DPP_2An(9,10)$ and $DPP_2An(2,6)$

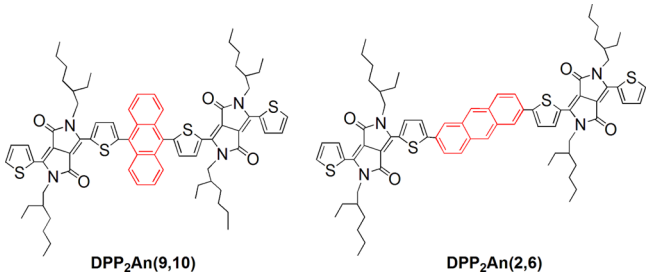

2. RESULTS AND DISCUSSION

2.1. Synthesis. The synthetic routes of two A-Ar-A-type SMs are depicted in Scheme 2. 3-(5-Bromothiophene-2-yl)-2,5-bis(2-ethylhexyl)-6-(thiophene-2-yl)pyrrolo[3,4-*c*]pyrrole-1,4-(2H,5H)dione[**DPP-Br**],[35] 9,10-bis(4,4,5,5-tetramethyl-1,3,2-dioxaborolan-2-yl)anthracene[**An(9, 10)B**],[25] and 2,6-bis-(4,4,5,5-tetramethyl-1,3,2-dioxaborolan-2-yl)anthracene [**An-(2,6)B**][36] were synthesized following the same procedures in the literature. $DPP_2An(9,10)$ and $DPP_2An(2,6)$ were obtained by Suzuki coupling reaction with a ~60% yield. Both new photovoltaic SMs were characterized by MS, ^{1}H NMR, and elemental analysis, which are consistent with their molecular structures. Furthermore, they displayed excellent solubililty in dichloromethane, chloroform, and dichlorobenzene at room temperature.

2.2. Thermal and Crystalline Properties. The thermal properties of $DPP_2An(9,10)$ and $DPP_2An(2,6)$ were characterized by thermogravimetric analyses (TGA) at a heating rate of 10 °C min^{-1} under N_2 atmosphere. The TGA curves are depicted in Figure 1, and their thermal parameters are summarized in Table 1. The thermal decomposition temperatures (T_d) of 418 °C for $DPP_2An(9,10)$ and 421 °C for $DPP_2An(2,6)$ are exhibited at a 5% weight loss. It indicates that

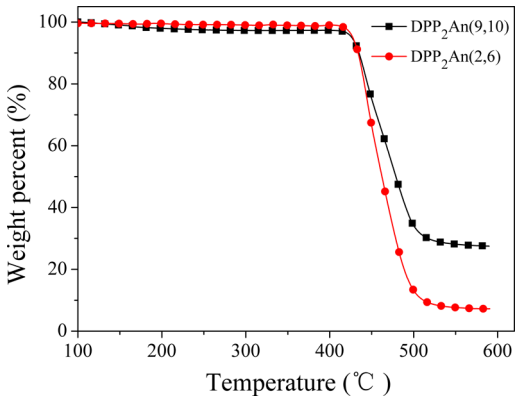

Figure 1. TGA curves of $DPP_2An(9,10)$ and $DPP_2An(2,6)$.

Scheme 2. Synthetic Route of $DPP_2An(9,10)$ and $DPP_2An(2,6)$

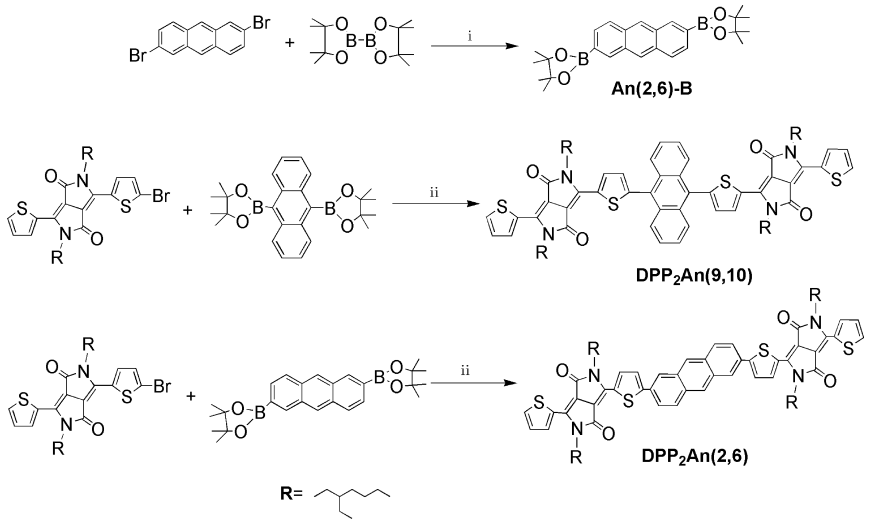

(i) 1,4-dioxane, KOAc, $PdCl_2(dppf)$, 60 °C; (ii) $Pd(PPh_3)_4$, toluene, 2 M potassium carbonate, CH_3CH_2OH, 110 °C.

DOI: 10.1021/acsami.5b03338
ACS Appl. Mater. Interfaces 2015, 7, 18292−18299

Table 1. Electrochemical and Thermal Parameters for $DPP_2An(9,10)$ and $DPP_2An(2,6)$

SMs	E_{ox}^{on} (V)	E_{red}^{on} (V)	E_{HOMO} (eV)[a]	E_{LUMO} (eV)[a]	E_g^{ec} (eV)[b]	T_d (°C)
$DPP_2An(9,10)$	1.11	−0.92	−5.38	−3.35	2.03	418
$DPP_2An(2,6)$	0.92	−1.02	−5.19	−3.25	1.94	421

[a]Calculated from the empirical equations: $E_{HOMO} = -(E_{ox}^{on} + 4.27)$ eV, $E_{LUMO} = -(E_{red}^{on} + 4.27)$ eV. [b]Calculated from $E_g^{ec} = -(E_{ox}^{on} - E_{red}^{on})$.

$DPP_2An(9,10)$ and $DPP_2An(2,6)$ have high thermal stability. Changing the substituted positions of the An core has little influence on the thermal stability for the A-Ar-A-type SMs.

Figure 2 depicts the differential scanning calorimetry (DSC) plots of both SMs in solid state. The typical endothermal peaks

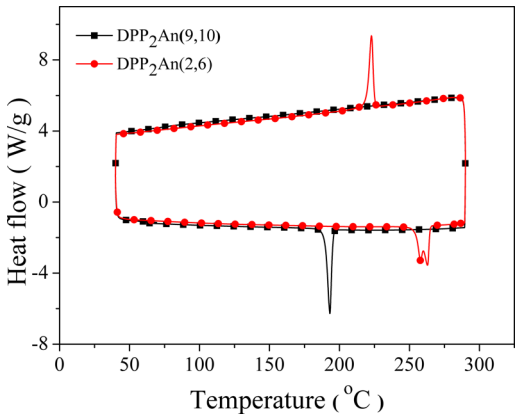

Figure 2. DSC plots of $DPP_2An(9,10)$ and $DPP_2An(2,6)$.

at 193 and 260 °C are observed for $DPP_2An(9,10)$ and $DPP_2An(2,6)$ during heating process, which correspond to melting temperatures (T_m), respectively. However, only $DPP_2An(2,6)$ displayed an exothermal peak at 223 °C during cooling process. It indicates that $DPP_2An(2,6)$ has the higher melting temperature, furthermore possessing better crystallinity than $DPP_2An(9,10)$. Thus, introducing 2,6-substituted instead of 9.10-substituted An core can enhance molecular crystallinity, further promoting $\pi-\pi$ stacking and charge transport.[31]

2.3. Electrochemical Properties. Cyclic voltammetry (CV) was employed to evaluate redox potentials and molecular orbital energy levels. The recorded CV plots of $DPP_2An(9,10)$ and $DPP_2An(2,6)$ on a platinum electrode are shown in Figure 3, and the electrochemical data are listed in Table 1, which were

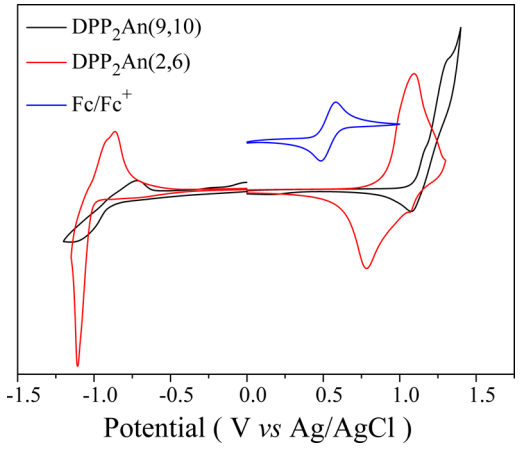

Figure 3. Cyclic voltammogram curves of $DPP_2An(9,10)$ and $DPP_2An(2,6)$.

measured in 0.1 M tetrabutylammonium hexafluorophosphate ($TBAPF_4$) solution (Bu_4NPF_6) of anhydrous acetonitrile (CH_3CN) at a scan rate of 100 mV/s.

It is found that both SMs undergo a reversible oxidation process and quasi-reversible reduction process. Similar oxidation and reduction behaviors were reported by Zaborova group.[37] The onset oxidation potential (E_{ox}^{on}) value is decreased from 1.11 to 0.92 V, and the onset reduction potential (E_{red}^{on}) value drops from −0.92 to −1.02 V for $DPP_2An(2,6)$ instead of DPP_2 An(9,10) vs Ag/AgCl. On the basis of the formal potential (0.53 V) of Fc/Fc^+ vs Ag/AgCl measured in this work and the reported energy level (−4.80 eV) of Fc/Fc^+ below the vacuum level, the HOMO and LUMO energy levels (E_{HOMO} and E_{LUMO}) of both SMs are calculated from the empirical equations shown in Table 1.[25] As a result, the HOMO/LUMO energy levels are −5.38 eV/−3.35 eV for $DPP_2An(9,10)$ and −5.19 eV/−3.25 eV for $DPP_2An(2,6)$. It is distinct that $DPP_2An(2,6)$ exhibits increasing HOMO and LUMO energy levels, as well as a decreasing electrochemical band gap (E_g^{ec}) compared to $DPP_2An(9,10)$, as it has better planarity and larger conjugation degree.

2.4. Optical Properties. The UV−vis absorption spectra of $DPP_2An(9,10)$ and $DPP_2An(2,6)$ in $CHCl_3$ solution and in their neat films are displayed in Figure 4. Their corresponding

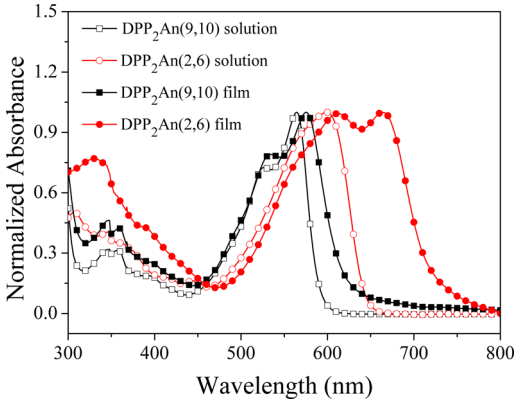

Figure 4. UV−vis absorption spectra of $DPP_2An(9,10)$ and $DPP_2An(2,6)$ in $CHCl_3$ and in their neat films.

absorption data are presented in Table 2. Two distinct absorption bands appeared for both SMs in solutions and their neat films. The high-lying band in the 300−400 nm region is attributed to the $\pi-\pi^*$ transition band, and the low-lying

Table 2. Optical Properties of $DPP_2An(9,10)$ and $DPP_2An(2,6)$

SMs	λ_{max} (nm) solution	λ_{max} (nm) film	λ_{onset} (nm) film	E_g^{opt} (eV)[a]
$DPP_2An(9,10)$	564	575	626	1.98
$DPP_2An(2,6)$	599	612, 662	726	1.71

[a]Calculated from the formula, $E_g^{opt} = 1240/\lambda_{onset}$

DOI: 10.1021/acsami.5b03338
ACS Appl. Mater. Interfaces 2015, 7, 18292−18299

band in the 450−700 nm region belongs to the intramolecular charge transfer (ICT) from the An core to the DPP moiety. These UV−vis absorption profiles are the typical feature of the D−A-type conjugated SMs.[38]

In contrast to $DPP_2An(9,10)$, $DPP_2An(2,6)$ exhibits a significantly bathochromic absorption peak in the $CHCl_3$ solution and in the solid film, respectively. Furthermore, $DPP_2An(2,6)$ displays a discernible vibronic shoulder peak in the low-lying region. It implies that $DPP_2An(2,6)$ has a larger conjugation system and better planar conformation, which result in more effective $\pi-\pi$ stacking in the solid state.[26] The optical band gaps (E_g^{opt}) of $DPP_2An(2,6)$ and DPP_2 An(9,10) are 1.71 and 1.98 eV, respectively, estimating from their film absorption band edges. It indicates that $DPP_2An(2,6)$ with lower E_g^{opt} value has more extended electron delocalization, caused by the smaller torsional angle between the An and DPP units.[39] Therefore, changing the substituted positions from the 9,10-positions to the 2,6-positions for the An core is beneficial to enhance the spectral absorption and decrease the optical band gaps.

2.5. Theoretical Calculation. Density functional theory (DFT) calculations were performed for both isomers of $DPP_2An(9,10)$ and $DPP_2An(2,6)$ at the B3LYP/6-31G(d) level using the Gaussian 09 program in order to get insight into their molecular geometry and electronic structures. To simplify the calculation, a 2-ethylhexyl unit attached to a nitrogen atom of the DPP unit was replaced by a methyl group. The simulated electron density distributions of the HOMO and LUMO, as well as the optimized lowest energy geometry are shown in Figure 5. Significantly different dihedral angles (left: D1 and right: D2) are observed between the An core and either thiophene unit next to anthracene. The dihedral angles are 58.47 ° and 65.63 ° for $DPP_2An(9,10)$, corresponding to 7.75 ° and 7.81° for DPP_2 An(2,6). It demonstrates that $DPP_2An(2,6)$ has better planar structure and increased interchain $\pi-\pi$ interaction as previously discussed, which can induce high crystallinity and good charge-transport properties, and further greatly improve J_{sc}.[40,41] On the basis of the electron density distributions of HOMOs and LUMOs for $DPP_2An(2,6)$ and $DPP_2An(9,10)$, we find that electron density is delocalized in the A-Ar-A skeleton for HOMOs. LUMOs exhibit an enhanced electron density located in molecular donor units, in contrast to HOMOs. However, it is different that the electron density is increased in an anthracene and two thienyl units for $DPP_2An(2,6)$, but a phenyl and two thienyl units for $DPP_2An(9,10)$. Therefore, $DPP_2An(2,6)$ has larger electron delocalization than $DPP_2An(9,10)$, which is consistent with the above absorption.

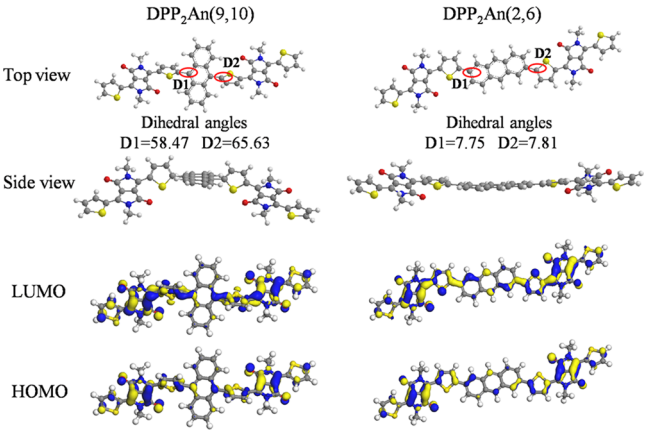

Figure 5. Molecular geometries and electron density distributions of HOMO and LUMO for $DPP_2An(9,10)$ and $DPP_2An(2,6)$.

2.6. Photovoltaic Properties. Solution-processed organic photovoltaic cells based on $DPP_2An(9,10)$ and $DPP_2An(2,6)$ were made with a device configuration of ITO/PEDOT:PSS (40 nm)/photoactive layer (80 nm)/Ca(10 nm)/Al(100 nm). The photoactive layer here was formed by spin-coating at a constant concentration of 12 mg/mL, comprising a mixture of SM and $PC_{71}BM$ in chloroform. The ratios between SM and $PC_{71}BM$ were changed from 1:1, 1:2, 1:3, 1:4 to 1:5 and 1:6 in order to optimize the ratio of $DPP_2An(9,10)/PC_{71}BM$ and $DPP_2An(2,6)/PC_{71}BM$. Moreover, concentrations of 1,8-diiodooctane (DIO) solvent additive were tuned from 0, 0.5%, and 1.0% to 1.5% in order to improve morphology of photoactive layer. The measured photovoltaic properties of these $DPP_2An(9,10)/PC_{71}BM$ and $DPP_2An(2,6)/PC_{71}BM$ based cells are listed in Table S1. It is demonstrates that the optimized processing conditions are different, in which the optimized $DPP_2An(9,10)/PC_{71}BM$ cell is made at a ratio of 1:5 without DIO additive, and the optimized $DPP_2An(2,6)/PC_{71}BM$ cell is fabricated at a ratio of 1:1 with 1% DIO additive. The resulting photovoltaic properties are presented in Table 3 at the optimized ratio and different DIO concentrations. Under these optimized conditions, the $DPP_2An(9,10)$-based cell exhibited a relatively high V_{oc} of 0.97 V, but a low PCE of 1.45% with a J_{sc} of 4.09 mA/cm^2 and an FF of 31.66%. In contrast, the $DPP_2An(2,6)$-based cell displayed significantly increased PCE of 5.44%, J_{sc} of 11.90 mA/cm^2, and FF of 55.40%, except for the decreasing V_{oc} of 0.82 V. Apparently, $DPP_2An(2,6)$ exhibited PCE, J_{sc}, and *FF* values considerably higher than $DPP_2An(9,10)$ in the cells. Figure 6 shows $J-V$ characteristics of the cells based on $DPP_2An(9,10)$ and $DPP_2An(2,6)$ under the optimized conditions. Compared to the reported DPP_2Ar-type SMs with the Ar hydrocarbon core, $DPP_2An(2,6)$ displayed the highest PCE value. Therefore, the properly enlarged conjugated system of the aryl core and the changing substituted positions from the 9,10-position to the

Table 3. Photovoltaic Properties of the Photovoltaic Cells with $DPP_2An(9,10)$ and $DPP_2An(2,6)$ at Optimized SMs/$PC_{71}BM$ Ratios under an Illumination of AM 1.5 G Solar Irradiance (100 mW cm^{-2})

photoactive layer	D/A [*w*/*w*]	DIO [*v*/*v* %]	J_{sc} [mA/cm^2]	V_{oc} [V]	*FF* [%]	PCE_{max} [%]	μ_h [cm^{2}v^{-1}s^{-1}]
$DPP_2An(9,10)/PC_{71}BM$	1:5	0	4.09	0.97	31.66	1.45	2.19×10^{-6}
	1:5	1.0	3.06	0.96	29.35	0.86	1.53×10^{-6}
$DPP_2An(2,6)/PC_{71}BM$	1:1	0	4.51	0.85	46.48	1.79	6.77×10^{-5}
	1:1	0.5	11.10	0.83	54.64	5.05	1.47×10^{-4}
	1:1	1.0	11.90	0.82	55.40	5.44	4.02×10^{-4}
	1:1	1.5	11.15	0.81	50.69	4.58	1.69×10^{-4}

DOI: 10.1021/acsami.5b03338
ACS Appl. Mater. Interfaces 2015, 7, 18292−18299

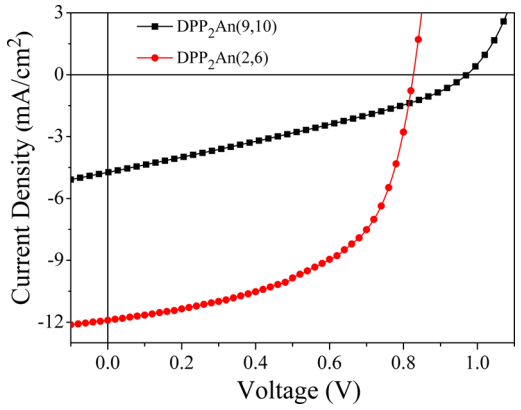

Figure 6. *J*–*V* curves of the photovoltaic cells with $DPP_2An(9,10)$ and $DPP_2An(2,6)$ at the optimized processing conditions under an illumination of AM 1.5 G solar irradiance (100 mW cm^{-2}).

2,6-position for the An core are available to enhance PCE for their SMs in OSCs.

To further understand why the $DPP_2An(2,6)$-based cell exhibited a higher J_{sc} value than the $DPP_2An(9,10)$-based cell, the external quantum efficiency (EQE) curve of their fabricated devices under the optimized processing conditions were measured as shown in Figure 7. A broad photoresponse region

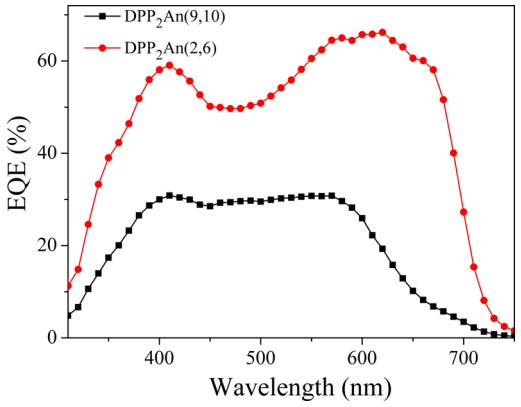

Figure 7. EQE curves of the photovoltaic cells with $DPP_2An(9,10)$ and $DPP_2An(2,6)$ at the optimized processing conditions.

from 300 to 750 nm is analogously observed in both cells. However, it is different that the $DPP_2An(2,6)$-based cell displays a significantly improved EQE of 66.2% compared to the $DPP_2An(9,10)$-based cell, in which the latter cell only shows a low EQE of 30.8%. A higher EQE level is suggested to be available for the $DPP_2An(2,6)/PC_{71}BM$-based devices to display higher J_{sc} values than the $DPP_2An(9,10)/PC_{71}BM$-based devices.

2.7. Molecular Stacking and Film Morphology. To further study the crystallinity and molecular stacking of the neat films for $DPP_2An(9,10)$ and $DPP_2An(2,6)$, as well as their photoactive layers at the optimized SMs/$PC_{71}BM$ ratios, X-ray diffraction (XRD) analyses were made. The recorded XRD plots are shown in Figure 8. Both neat films and the other $DPP_2An(9,10)/PC_{71}BM$ blending films at a ratio of 1:5 with/without DIO additive only exhibit a sharp diffraction peak in the small-angle region ($2\theta < 5°$).

However, the $DPP_2An(2, 6)/PC_{71}BM$ blending film exhibits a series of sharp diffraction peaks in the small-angle and wide-

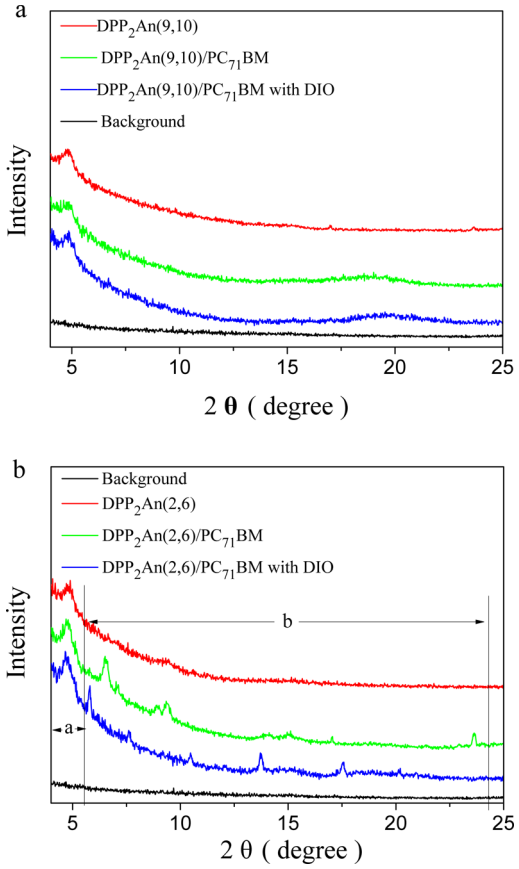

Figure 8. XRD plots of the neat and blended films with $DPP_2An(9,10)$ (a); and $DPP_2An(2,6)$ (b).

angle regions at a ratio of 1:1 with/without 1% DIO additive. Furthermore, this blending film with 1% DIO additive displays more diffraction peaks. These diffraction peaks are attributed to the orientation along the direction of the alkyl chains in the small-angle region and backbone stacking in the wide-angle region, respectively. It indicates that the $DPP_2An(2,6)/PC_{71}BM$-blending film with DIO additive has the highest ordered diffractions among these neat films and blend films, and that the domains between donor and acceptor were well formed.[31] Therefore, DIO additive is favored to promote $DPP_2An(2,6)$ to exhibit better crystallinity and network, which can further improve carrier transport.[42]

In order to further explore the influence of the DIO additive on the film morphology of the blend films, their morphologies were recorded with transmission electron microscopy (TEM). Figure 9 shows the TEM images of the $DPP_2An(2,6)/PC_{71}BM$ (1:1) and $DPP_2An(9,10)/PC_{71}BM$ (1:5) blend films with/without 1% DIO additive. It demonstrates that the DIO additive gives almost no influence on the morphology of the $DPP_2An(9,10)/PC_{71}BM$ blend film. However, some dark regions are observed in the $DPP_2An(2,6)/PC_{71}BM$ blend film without the DIO additive, which are suggested to be the presence of large $PC_{71}BM$ domains. As these domain sizes are far larger than the exciton diffusion lengths (~10 nm), it has the potential to hinder exciton dissociation.[43] While the $DPP_2An(2,6)/PC_{71}BM$ (1:1) film is processed with 1% DIO additive, a significantly more homogeneous morphology with a fiber-like structure appears, meaning that a continuously interpenetrated network is formed, which is favorable for the charge transportation.[44] Therefore, adding DIO additive can

DOI: 10.1021/acsami.5b03338
ACS Appl. Mater. Interfaces 2015, 7, 18292–18299

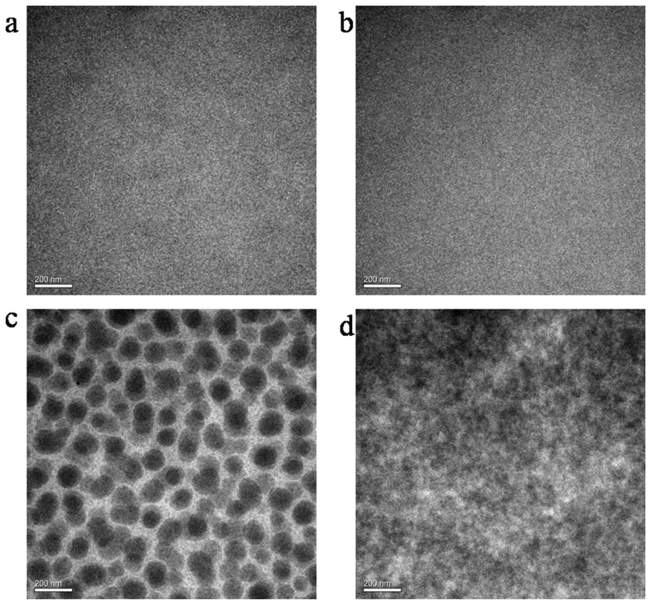

Figure 9. TEM images of the $DPP_2An(9,10)/PC_{71}BM$ (1:5) films without/with 1% DIO additive (a, b); the $DPP_2An(2,6)/PC_{71}BM$ (1:1) films without/with 1% DIO additive (c, d).

significantly improve the crystalline order and eventually enhance the p-type domain connectivity.[45,46] As a result, the device performance can be improved in the $DPP_2An(2,6)/PC_{71}BM$-based solar cell.

2.8. Hole Mobility. The hole mobilities of $DPP_2An(9,10)$ and $DPP_2An(2,6)$ were measured in their hole-only devices with a structure of ITO/PEDOT:PSS/SM:$PC_{71}BM$/Au using the space charge limited current (SCLC) method. The measured $J-V$ curves of these hole-only devices at different DIO ratios and the optimized hole-only devices in the dark are shown in Figure S1 and Figure 10, respectively. On the basis of

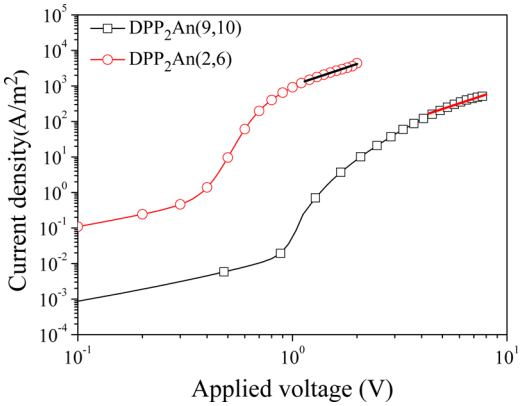

Figure 10. $J-V$ characteristics of the optimized hole-only $DPP_2An(9,10)$ and $DPP_2An(2,6)$ devices.

the reported equation: $J = (9/8)\varepsilon_0\varepsilon_r\mu h(V/L^3)$,[47] the calculated holes mobilities are also listed in Table 3 for comparison. It is observed that the small molecular structure, as well as the SM/$PC_{71}BM$ ratios and DIO concentrations have significant influence on holes mobility of $DPP_2An(2,6)$ and $DPP_2An(9,10)$. Higher holes mobilities of 2.19×10^{-6} cm^2 v^{-1} s^{-1} and 4.02×10^{-4} cm^2 v^{-1} s^{-1} are exhibited in the $DPP_2An(9,10)/PC_{71}BM$-based device at a 1:5 ratio without the DIO additive and the $DPP_2An(2,6)/PC_{71}BM$-based device at a 1:1 ratio with 1% DIO additive, respectively. It is obvious that the holes mobility of $DPP_2An(2,6)$ is two orders of magnitude higher than that of $DPP_2An(9,10)$ in the optimized hole-only devices. Therefore, $DPP_2An(2,6)$ displayed higher *FF* value than $DPP_2An(9,10)$ in the cells.

3. CONCLUSIONS

In conclusion, two isomeric A-Ar-A-type SMs of $DPP_2An(9,10)$ and $DPP_2An(2,6)$ were obtained. Significantly improved optoelectronic and photovoltaic properties were observed from $DPP_2An(9,10)$ to $DPP_2An(2,6)$. The highest hole mobility of 4.02×10^{-4} cm^2 v^{-1} s^{-1} was presented in the hole-only $DPP_2An(2,6)$-based devices, which is 2 orders of magnitude higher than that in the hole-only $DPP_2An(9,10)$ based one. Moreover, the solution-processing solar cells containing $DPP_2An(2,6)$ and $PC_{71}BM$ (1:1) with 1% DIO additive exhibited increasing PCE of 5.44% and J_{sc} of 11.90 mA/cm^2 and FF of 55.40%. The PCE and FF values were 3.7 and 2.9 times those of the $DPP_2An(9,10)$-based solar cells, respectively. It was concluded that the enlarging conjugated system of the An core and changing its substituted positions from the 9,10-positions to the 2,6-positions in the A-Ar-A-type SMs can obviously improve the optoelectronic and photovoltaic properties for their corresponding SMs.

4. EXPERIMENTAL SECTION

Synthesis. All reactions were made under nitrogen atmosphere. All solvents and reagents were purchased from Sigma, Aldrich, and Adamas. These chemicals were used without purification unless stated otherwise. Toluene was distilled from sodium-benzophenone under nitrogen atmosphere prior to use.

Measurement and Characterization. ^1H NMR spectra were measured at 400 MHz on a Bruker Avance-400 spectrometer using $CDCl_3$ as a solvent and TMS (tetramethylsilane) as an internal standard. Mass spectra were made on a Bruker Daltonics BIFLEX III MALDI-TOF analyzer. UV−vis absorption spectra were recorded on a Shimadzu UV-1800 spectrophotometer. TGA was measured on a PerkinElmer Diamond TG/DTA thermal analyzer. Cyclic voltammetry was performed on a CHI620 voltammetric analyzer using 0.1 M Bu_4NPF_6 solution in anhydrous CH_3CN as electrolyte under argon atmosphere. A platinum disk and a platinum wire were used as working electrode and counter electrode, respectively. An Ag/AgCl electrode was employed as reference electrode. $DPP_2An(9,10)$ and $DPP_2An(2,6)$ were coated on the platinum disk surface and all potentials were corrected against Fc/Fc^+.

Synthesis of 2,6-Bis(4,4,5,5-tetramethyl-1,3,2-dioxaborolan-2-yl)anthracene (An(2,6)B). Bis(pinacolato) diboron (499 mg, 1.96 mmol), 2,6-dibromoanthracene (300 mg, 0.89 mmol), potassium acetate (523 mg, 5.34 mmol), and [1,10-bis(diphenylphosphino)-ferrocene]dichloropalladium [$PdCl_2$(dppf)] (22 mg, 0.03 mmol) and 1,4-dioxane (20 mL) were added into a 50 mL three-necked flask. The mixture was degassed for 30 min under nitrogen flow and then stirred at 60 °C for 24 h under nitrogen atomosphere. After being cooled down to ambient temperature, the reaction mixture was extracted with dichloromethane (DCM, 3 × 20 mL). The organic layer was collected and dried over anhydrous magnesium sulfate. The dried organic solution was filtered and distilled by rotary evaporation. The resulting residue was purified on a flash silica gel column using a mixing solvents of petroleum ether (PE) and DCM (*V*/*V*, 2:1) as eluent to afford a yellow solid (185 mg, yield 48.2%). ^1H NMR (400 MHz, $CDCl_3$) δ ppm, 8.55 (s, 2H), 8.44 (s, 2H), 7.99 (d, J = 8.0 Hz, 2H), 7.78 (d, J = 8.0 Hz, 2H), and 1.41 (s, 24H). MALDI-MS(m/z): 430.274 for $[M]^+$.

Synthesis of $DPP_2An(9,10)$. DPPBr (200 mg, 0.33 mmol), An(9,10)B (72 mg, 0.17 mmol), 2 M potassium carbonate (K_2CO_3, 2 mL), tetrakis(triphenylphosphine) palladium ($Pd(PPh_3)_4$) (19 mg, 0.02 mmol), and toluene (10 mL) was added into a 50 mL three-necked flask and degassed for 30 min with nitrogen flow. The mixture

DOI: 10.1021/acsami.5b03338
ACS Appl. Mater. Interfaces 2015, 7, 18292−18299

was stirred and refluxed at 110 °C for 24 h under the nitrogen protection. After being cooled down to ambient temperature, the reaction mixture was poured into the solution of methanol (200 mL) and hydrochloric acid (10 mL) with stirring to get precipitation. The precipitation was collected and purified on silica gel column using $CHCl_3$ as eluent to provide $DPP_2An(9,10)$ as a wine-colored solid (130 mg, 63.4% yield). ^1H NMR (400 MHz, $CDCl_3$) δ ppm, 9.22 (s, 2H), 8.95 (s, 2H), 7.49−7.95 (m, 4H), 7.66 (d, J = 4.0 Hz, 2H), 7.47−7.49 (m, 4H), 7.42 (s, 2H), 7.30 (s, 2H), 4.03−4.14 (m, 8H), 1.95 (d, J = 26.4 Hz, 4H), 1.22−1.36 (m, 32H), and 0.88−0.93 (m, 24H). MALDI-MS (m/z): 1223.656 for $[M]^+$. Anal. Calcd. for $C_{74}H_{86}N_4O_4S_4$: C, 72.56; H, 7.02; N, 4.58; S, 10.45. Found: C, 72.50; H, 7.05; N, 4.53; S, 10.17.

Synthesis of $DPP_2An(2,6)$. $DPP_2An(2,6)$ was prepared referred to the above synthetic procedure of $DPP_2An(9,10)$. When DPPBr (200 mg, 0.33 mmol) was reacted with An(2,6)-B (72 mg, 0.17 mmol) in the presence of 2 M K_2CO_3 (2 mL) and $Pd(PPh_3)_4$ (19 mg, 0.02 mmol), $DPP_2An(2,6)$ was obtained as a deep blue solid (120 mg, 57.7% yield). ^1H NMR (400 MHz, $CDCl_3$) δ ppm, 8.96 (d, J = 38.84 Hz, 4H), 8.34 (s, 2H), 8.16 (s, 2H), 7.99 (d, J = 4.0 Hz, 2H), 7.74 (d, J = 4.0 Hz, 2H), 7.59 (s, 4H), 7.25 (s, 2H), 4.04 (d, J = 15.3 Hz, 8H), 1.91 (d, J = 32.5 Hz, 4H), 1.32(dd, J = 27.6 Hz, 32H), 0.90 (d, J = 7.0 Hz, 24H). MALDI-MS(m/z): 1223.712 for $[M]^+$. Anal. Calcd. for $C_{74}H_{86}N_4O_4S_4$: C, 72.56; H, 7.02; N, 4.58; S, 10.45. Found: C, 72.30; H, 7.25; N, 4.53; S, 10.31.

Fabrication and Characterization of Photovoltaic Cells. Indium tin oxide (ITO)-coated glass substrates were successively cleaned by ultrason wave with detergent, deionized water, acetone, and isopropyl alcohol each for 20 min. Poly(3,4-ethylene dioxythiophene)/poly(styrenesulfonate) (PEDOT:PSS, Clevios P Al 4083) was spin-coated onto ITO glass and baked at 150 °C for 10 min in air. The photoactive layer was formed by spin-coating a blend chloroform solution of SMs/$PC_{61}BM$ (or $PC_{71}BM$) onto PEDOT:PSS layer. Ca (10 nm) and Al (100 nm) were successively deposited on a photoactive layer by thermal evaporation at a vacuum of 1×10^{-6} mbar. The J−V characteristics were performed under Newport 150 W solar simulator with an irradiation intensity of 100 mW/cm^2. The EQE curves of the devices were performed on QE-R3011 of solar cell spectral response measurement system (Enli Technology). Film morphologies were recorded on the Tecnai G2 F20 S-TWIN TEM under an acceleration voltage of 100 kV, in which the active-films were made using a special processing technique.[31] First, the active-films were spin-cast on the PEDOT:PSS/ITO substrates. Second, the resulting active-film/PEDOT:PSS/ITO substrates were submerged in deionized water to make these active-films float onto the air−water interface. Finally, the floated active-films were taken up on unsupported 200 mesh copper grids for a TEM measurement.

■ ASSOCIATED CONTENT

Supporting Information

The Supporting Information is available free of charge on the ACS Publications website at DOI: 10.1021/acsami.5b03338.

^1H NMR spectra, mass spectra, table of photovoltaic properties for the solar cells, and figures of J−V characteristics for the hole-only devices (PDF)

■ AUTHOR INFORMATION

Corresponding Authors

*Tel: +86-731-58293377; fax: +86-731-58292051; e-mail: yangrq@qibebt.ac.cn (R.Y.).

*Tel: +86-731-58293377; fax: +86-731-58292051; e-mail: zhuwg18@126.com (W.Z.).

Notes

The authors declare no competing financial interest.

■ ACKNOWLEDGMENTS

The authors are thankful for the financial support of the Major Cultivation and General Programs of the National Natural Science Foundation of China (91233112, 21172187, 51403178), the Program for Innovative Research Cultivation Team in University of Ministry of Education of China (1337304), the Innovation Group in Hunan Natural Science Foundation (12JJ7002), the Natural Science Foundation of Hunan (14JJ4019, 2015JJ3113), Open Project for the National Key Laboratory of Luminescent Materials and Devices (2014-skllmd-10), Research Foundation of Hunan Education Bureau (13A102, 14C1099), the Hunan Postgraduate Science Foundation for Innovation (CX- 2014B257), and the Natural Science Foundation of Xiangtan University (13QDZ23).

■ REFERENCES

(1) Li, Z.; Dong, Q.; Li, Y.; Xu, B.; Deng, M.; Pei, J.; Tian, W. Design and Synthesis of Solution Processable Small Molecules Towards High Photovoltaic Performance. *J. Mater. Chem.* **2011**, *21*, 2159−2168.

(2) Roncali, J. Molecular Bulk Heterojunctions: an Emerging Approach to Organic Solar Cells. *Acc. Chem. Res.* **2009**, *42*, 1719−1730.

(3) Walker, B.; Kim, C.; Nguyen, T. Q. Small Molecule Solution-Processed Bulk Heterojunction Solar Cells. *Chem. Mater.* **2011**, *23*, 470−482.

(4) Chen, Y.; Wan, X.; Long, G. Y. High Performance Photovoltaic Applications Using Solution-Processed Small Molecules. *Acc. Chem. Res.* **2013**, *46*, 2645−2655.

(5) Liu, J.; Zhang, Y.; Phan, H.; Sharenko, A.; Moonsin, P.; Walker, B.; Promarak, V.; Nguyen, T. Q. Effects of Stereoisomerism on the Crystallization Behavior and Optoelectrical Properties of Conjugated Molecules. *Adv. Mater.* **2013**, *25*, 3645−3650.

(6) Li, Y.; Guo, Q.; Li, Z.; Pei, J.; Tian, W. Y. Solution Processable D-A Small Molecules for Bulk-Heterojunction Solar Cells. *Energy Environ. Sci.* **2010**, *3*, 1427−1436.

(7) Kan, B.; Li, M.; Zhang, Q.; Liu, F.; Wan, X.; Wang, Y.; Chen, Y. A Series of Simple Oligomer-like Small Molecules Based on Oligothiophenes for Solution-Processed Solar Cells with High Efficiency. *J. Am. Chem. Soc.* **2015**, *137*, 3886−3893.

(8) Jheng, J. F.; Lai, Y. Y.; Wu, J. S.; Chao, Y. H.; Wang, C. L.; Hsu, C. S. Influences of the Non-Covalent Interaction Strength on Reaching High Solid-State Order and Device Performance of a Low Bandgap Polymer with Axisymmetrical Structural Units. *Adv. Mater.* **2013**, *25*, 2445−2451.

(9) Lindgren, L. J.; Zhang, F.; Andersson, M.; Barrau, S.; Hellstrom, S.; Mammo, W.; Perzon, E.; Inganas, O.; Andersson, M. R. Synthesis, Characterization, and Devices of a Series of Alternating Copolymers for Solar Cells. *Chem. Mater.* **2009**, *21*, 3491−3502.

(10) Warnan, J.; Cabanetos, C.; Labban, A. E.; Hansen, M. R.; Tassone, C.; Toney, M. F.; Beaujuge, P. M. Ordering Effects in Benzo[1,2-b:4,5-b′]difuran-thieno[3,4-c]pyrrole-4,6- dione Polymers with > 7% Solar Cell Efficiency. *Adv. Mater.* **2014**, *26*, 4357−4362.

(11) Meager, I.; Ashraf, R. S.; Mollinger, S.; Schroeder, B. C.; Bronstein, H.; Beatrup, D.; Vezie, M. S.; Kirchartz, T.; Salleo, A.; Nelson, J.; McCulloch, I. Photocurrent Enhancement from Diketo-pyrrolopyrrole Polymer Solar Cells through Alkyl-Chain Branching Point Manipu- lation. *J. Am. Chem. Soc.* **2013**, *135*, 11537−11540.

(12) Zerdan, R. B.; Shewmon, N. T.; Zhu, Y.; Mudrick, J. P.; Chesney, K. J.; Xue, J.; Castellano, R. K. The Influence of Solubilizing Chain Stereochemistry on Small Molecule Photovoltaics. *Adv. Funct. Mater.* **2014**, *24*, 5993−6004.

(13) Shi, J.; Zhao, W.; Xu, L.; Kan, Y.; Li, C.; Song, J.; Wang, H. Small Molecules of Cyclopentadithiophene Derivatives: Effect of Sulfur Atom Position and Substituted Groups on Their UV-Abs Properties. *J. Phys. Chem. C* **2014**, *118*, 7844−7855.

(14) Takacs, C. J.; Sun, Y.; Welch, G. C.; Perez, L. A.; Liu, X.; Wen, W.; Bazan, G. C.; Heeger, A. J. Solar Cell Efficiency, Self-Assembly,

DOI: 10.1021/acsami.5b03338
ACS Appl. Mater. Interfaces 2015, 7, 18292−18299

and Dipole-Dipole Interactions of Isomorphic Narrow-Band-Gap Molecules. *J. Am. Chem. Soc.* **2012**, *134*, 16597−16606.
(15) Li, S.; He, Z.; Yu, J.; Zhong, A.; Tang, R.; Wu, H. B.; Qin, J. G.; Li, Z. How the Linkage Positions Affect the Performance of Bulk-Heterojunction Polymer Solar Cells. *J. Mater. Chem.* **2012**, *22*, 12523−12531.
(16) Lin, Y.; Ma, L.; Li, Y.; Liu, Y.; Zhu, D.; Zhan, X. A Solution-Processable Small Molecule Based on Benzodithiophene and Diketopyrrolopyrrole for High-Performance Organic Solar Cells. *Adv. Energy Mater.* **2013**, *3*, 1166−1170.
(17) Lin, Y.; Li, Y.; Zhan, X. A Solution-Processable Electron Acceptor Based on Dibenzosilole and Diketopyrrolopyrrole for Organic Solar Cells. *Adv. Energy Mater.* **2013**, *3*, 724−728.
(18) Qiao, Y.; Guo, Y.; Yu, C.; Zhang, F.; Xu, W.; Liu, Y.; Zhu, D. Diketopyrrolopyrrole- Containing Quinoidal Small Molecules for High-Performance, Air-Stable, and Solution- Processable n-Channel Organic Field-Effect Transistors. *J. Am. Chem. Soc.* **2012**, *134*, 4084−4087.
(19) Shin, W.; Yasuda, T.; Watanabe, G.; Yang, Y. S.; Adachi, C. Self-Organizing Mesomorphic Diketopyrrolopyrrole Derivatives for Efficient Solution-Processed Organic Solar Cells. *Chem. Mater.* **2013**, *25*, 2549−2556.
(20) Chen, T. L.; Zhang, Y.; Smith, P.; Tamayo, A.; Liu, Y.; Ma, B. Diketopyrrolopyrrole- Containing Oligothiophene-Fullerene Triads and Their Use in Organic Solar Cells. *ACS Appl. Mater. Interfaces* **2011**, *3*, 2275−2280.
(21) Murphy, L.; Hong, W.; Aziz, H.; Li, Y. Influences of Using a High Mobility Donor Polymer on Solar Cell Performance. *Org. Electron.* **2013**, *14*, 3484−3492.
(22) Schmidt, K.; Tassone, C. J.; Niskala, J. R.; Yiu, A. T.; Lee, O. P.; Weiss, T. M.; Toney, M. F. A Mechanistic Understanding of Processing Additive-Induced Efficiency Enhancement in Bulk Heterojunction Organic Solar Cells. *Adv. Mater.* **2014**, *26*, 300−305.
(23) Lim, B.; Yeo, J. S.; Khim, D.; Kim, D. Y. Synthesis and Photovoltaic Properties of a Thien- ylenevinylene and Diketopyrrolopyrrole Copolymer with High Mobility. *Macromol. Rapid Commun.* **2011**, *32*, 1551−1556.
(24) Chen, J.; Xiao, M.; Meng, F.; Duan, L.; Tan, H.; Wang, Y.; Zhu, W. Improving Photovoltaic Properties of Linear Small Molecules with TPA-DPP Segment by Tuning Their Frameworks. *Synth. Met.* **2015**, *199*, 400−407.
(25) Zhang, Y.; Bao, X.; Xiao, M.; Tan, H.; Tao, Q.; Wang, Y.; Zhu, W. Significantly Improved Photovoltaic Performance of the Triangular-spiral TPA(DPP-PN)$_3$ by Appending Planar Phenanthrene Units into the Molecular Terminals. *J. Mater. Chem. A* **2015**, *3*, 886−893.
(26) Zhang, Y.; Tan, H.; Xiao, M.; Bao, X.; Tao, Q.; Wang, Y.; Zhu, W. D-A-Ar-type Small Molecules with Enlarged π-system of Phenanthrene at Terminal for High-Performance Solution Processed Organic Solar Cells. *Org. Electron.* **2014**, *15*, 1173−1183.
(27) Lee, J. W.; Choi, Y. S.; Jo, W. H. Diketopyrrolopyrrole-based Small Molecules with Simple Structure for High V_{oc} Organic Photovoltaics. *Org. Electron.* **2012**, *13*, 3060−3066.
(28) Choi, Y. S.; Jo, W. H. A Strategy to Enhance Both V_{oc} and J_{sc} of A-D-A Type Small Molecules Based on Diketopyrrolopyrrole for High Efficient Organic Solar Cells. *Org. Electron.* **2013**, *14*, 1621−1628.
(29) Wong, W. W.; Subbiah, J.; Puniredd, S. R.; Purushothaman, B.; Pisula, W.; Kirby, N.; Holmes, A. B. Liquid Crystalline Hexa-peri-hexabenzocoronene-diketopyrrolopyrrole Organic Dyes for Photovoltaic Applications. *J. Mater. Chem.* **2012**, *22*, 21131−21137.
(30) Loser, S.; Miyauchi, H.; Hennek, J. W.; Smith, J.; Huang, C.; Facchetti, A.; Marks, T. J. A "zig-zag" Naphthodithiophene Core for Increased Efficiency in Solution-Processed Small Molecule Solar Cells. *Chem. Commun.* **2012**, *48*, 8511−8513.
(31) Huang, J.; Zhan, C.; Zhang, X.; Zhao, Y.; Lu, Z.; Jia, H.; Yao, J. Solution-processed DPP-based Small Molecule that Gives High Photovoltaic Efficiency With Judicious Device Optimization. *ACS Appl. Mater. Interfaces* **2013**, *5*, 2033−2039.
(32) Loser, S.; Bruns, C. J.; Miyauchi, H.; Ortiz, R. P.; Facchetti, A.; Stupp, S. I.; Marks, T. J. A Naphthodithiophene-Diketopyrrolopyrrole Donor Molecule for Efficient Solution-processed Solar Cells. *J. Am. Chem. Soc.* **2011**, *133*, 8142−8145.
(33) Harschneck, T.; Zhou, N.; Manley, E. F.; Lou, S. J.; Yu, X.; Butler, M. R.; Marks, T. J. Substantial Photovoltaic Response and Morphology Tuning in Benzo[1, 2-b: 6, 5-b′] dithiophene (bBDT) Molecular Donors. *Chem. Commun.* **2014**, *50*, 4099−4101.
(34) Jung, M.; Seo, D.; Kwak, K.; Kim, A.; Cha, W.; Kim, H.; Kim, B. Structural and Morphological Tuning of Dithienobenzodithiophene-core Small Molecules for Efficient Solution Processed Organic Solar Cells. *Dyes Pigm.* **2015**, *115*, 23−34.
(35) Shin, J.; Kang, N. S.; Lee, T. W.; Cho, M. J.; Hong, J. M.; Ju, B. K.; Choi, D. H. Two-Dimensional π-Conjugated Molecules Based-on 2,6,9,10-Tetra(prop-1-yn-1-yl)anthra- cene and Their Application to Solution-Processed Photovoltaic Cells. *Org. Electron.* **2014**, *15*, 1521−1530.
(36) Zhang, Y.; Kim, C.; Lin, J.; Nguyen, T. Q. Solution-Processed Ambipolar Field-Effect Transistor Based on Diketopyrrolopyrrole Functionalized with Benzothiadiazole. *Adv. Funct. Mater.* **2012**, *22*, 97−105.
(37) Zaborova, E.; Chávez, P.; Bechara, R.; Lévêque, P.; Heiser, T.; Méry, S.; Leclerc, N. Thiazole as a Weak Electron-Donor Unit to Lower the Frontier Orbital Energy Levels of Donor− Acceptor Alternating Conjugated Materials. *Chem. Commun.* **2013**, *49*, 9938−9940.
(38) Shin, M. G.; Kim, S. O.; Park, H. T.; Park, S. J.; Yu, H. S.; Kim, Y. H.; Kwon, S. K. Synthesis and Characterization of Ortho-twisted Asymmetric Anthracene Derivatives for Blue Organic Light Emitting Diodes (OLEDs). *Dyes Pigm.* **2012**, *92*, 1075−1082.
(39) Henson, Z. B.; Welch, G. C.; van der Poll, T.; Bazan, G. C. Pyridalthiadiazole-Based Narrow Band Gap Chromophores. *J. Am. Chem. Soc.* **2012**, *134*, 3766−3779.
(40) Liu, Z.; Zhang, G.; Cai, Z.; Chen, X.; Luo, H.; Li, Y.; Zhang, D. New Organic Semi- conductors with Imide/Amide Containing Molecular Systems. *Adv. Mater.* **2014**, *26*, 6965−6977.
(41) Son, H. J.; He, F.; Carsten, B.; Yu, L. Are We There Yet Design of Better Conjugated Polymers for Polymer Solar Cells. *J. Mater. Chem.* **2011**, *21*, 18934−18945.
(42) Liu, S. Y.; Liu, W. Q.; Xu, J. Q.; Fan, C. C.; Fu, W. F.; Ling, J.; Chen, H. Z. Pyrene and Diketopyrrolopyrrole-Based Oligomers Synthesized via Direct Arylation for OSC Applicat- ions. *ACS Appl. Mater. Interfaces* **2014**, *6*, 6765−6775.
(43) Proctor, C. M.; Kuik, M.; Nguyen, T. Q. Charge Carrier Recombination in Organic Solar Cells. *Prog. Polym. Sci.* **2013**, *38*, 1941−1960.
(44) Dang, D.; Chen, W.; Yang, R.; Zhu, W.; Mammo, W.; Wang, E. Fluorine Substitution Enhanced Photovoltaic Performance of a D−A1−D−A2 Copolymer. *Chem. Commun.* **2013**, *49*, 9335−9337.
(45) Chen, D.; Liu, F.; Wang, C.; Nakahara, A.; Russell, T. P. Bulk Heterojunction Photovoltaic Active Layers via Bilayer Interdiffusion. *Nano Lett.* **2011**, *11*, 2071−2078.
(46) Zhang, Q.; Kan, B.; Liu, F.; Long, G.; Wan, X.; Chen, X.; Chen, Y. Small-Molecule Solar Cells with Efficiency over 9%. *Nat. Photonics* **2014**, *9*, 35−41.
(47) Zhou, P.; Dang, D. F.; Xiao, M. J.; Wang, Q.; Zhong, J.; Tan, H.; Pei, Y.; Yang, R. Q.; Zhu, W. G. Improved Photovoltaic Performance of Star-shaped Molecules with a Triphenylamine Core by Tuning the Substituted Position of the Carbazolyl Unit at the Terminal. *J. Mater. Chem. A* **2015**, *3*, 10883−10889.

DOI: 10.1021/acsami.5b03338
ACS Appl. Mater. Interfaces 2015, 7, 18292−18299